Kinetic simulation of direct-current driven microdischarges in argon at atmospheric pressure

Reference:

Zhang Ya, Jiang Wei, Bogaerts Annemie.- Kinetic simulation of direct-current driven microdischarges in argon at atmospheric pressure

Journal of physics: D: applied physics - ISSN 0022-3727 - 47:43(2014), 435201

DOI: http://dx.doi.org/doi:10.1088/0022-3727/47/43/435201

Handle: http://hdl.handle.net/10067/1191520151162165141

Kinetic simulation of direct-current driven microdischarges in argon at atmospheric pressure

Ya Zhang[1,2], Wei Jiang[2,3], Annemie Bogaerts[1]
[1] *Research group PLASMANT, Department of Chemistry University of Antwerp, B-2610 Wilrijk-Antwerp, Belgium*
[2] *School of Physics, Huazhong University of Science and Technology, Wuhan 430074, China and*
[3] *Centre for Mathematical Plasma-Astrophysics, Department of Mathematics, Katholieke Universiteit Leuven, B-3001 Leuven, Belgium**

A one-dimensional, implicit particle-in-cell Monte Carlo collision model is used to simulate the plasma kinetic properties at steady state in a parallel-plate direct current argon glow microdischarge under various operating conditions, such as driving voltage ($30-1000$ V) and gap size ($10-1000$ μm) at atmospheric pressure. First, a comparison between rf and dc modes is shown for the same pressure, driving voltage and gap spacing. Furthermore, the effect of gap size scaling (in the range of $10-1000$ μm) on the breakdown voltage, peak electron density and peak electron current density at breakdown voltage is examined. The breakdown voltage is lower than 150 V in all gaps considered. The microdischarge is found to have a neutral bulk plasma region and a cathode sheath region with size varying with the applied voltage and the discharge gap. In our calculations, the electron and ion densities are of the order of $10^{18}-10^{23}$ m^{-3}, which is in the glow discharge limit, as the ionization degree is lower than1%. The electron energy distribution function (EEDF) shows a two-energy group distribution at a gap of 10 μm, and a three-energy group distribution at larger gaps such as 200 and 1000 μm, emphasizing the importance of the gap spacing in dc microdischarges.

PACS numbers:

I. INTRODUCTION

Microdischarges (MDs) are gas discharge plasmas generated in small dimensions, typically 100's of μm, and operating at gas pressures up to atmospheric pressure[1,2]. In recent years there has been a great research interest in atmospheric pressure non-equilibrium plasmas in MDs[3,4]. The reason is that atmospheric pressure MDs can produce stable, self-sustaining non-equilibrium glow-like plasmas in microgaps and offer a wide variety of potential applications that exploit their small length and high pressure properties, such as light sources, material processing and synthesis, chemical analysis, environmental applications, combustion and medical treatments[5,6].

There have been considerable efforts to develop MD devices that can effectively generate and maintain stable discharges at atmospheric pressure[2]. Different types of atmospheric pressure MDs, based on the power source, have been studied, such as direct current (dc) glow discharges[1,7], alternating current (ac) discharges[8], radio-frequency (rf) discharges[9], nanosecond-pulsed discharges[10] and microwave discharges[11]. dc glow discharges are of special interest due to their simplicity and stable operation conditions over a wide range of controllable parameters[12].

Atmospheric pressure dc glow discharges can be generated in a stable way between two electrodes, i.e., the transition to an unstable arc discharge can be avoided, when the electrode separation is kept below 1 mm[13]. However, experimental diagnostics of these MDs are very challenging, due to the small dimensions. Recent interest in dc MDs is motivated not only by the basic plasma physics[2] but also by the industrial applications[14,15], e.g., in microreactors for gas reforming, material deposition and the destruction of environmentally harmful substances. There have been many experimental investigations on dc MDs by using optical emission spectroscopy (OES)[7,13,16–18], laser Thomson scattering (LTS) and diode laser absorption spectroscopy[19]. Yokoyama et al. demonstrated by using OES that an atmospheric dc microplasma could be generated in air with a low gas flow of helium or argon through a nozzle, i.e., a glow discharge is observed with a positive column and a layered structure near the cathode[7]. Based on OES, atmospheric pressure dc glow discharges were investigated[13] between a thin cylindrical anode and a flat cathode with an inter-electrode gap spacing in the range of 20 μm-1.5 cm. Again, OES detection of a dc glow discharge was performed in a planar glass microstructure at close to atmospheric pressure using argon as a carrier gas[16]. Furthermore, OES was used to study an atmospheric pressure dc helium MD across a 200 μm slot[17], with a bulk electron density of about 10^{19} m^{-3}, as well as a 600 μm slot-type argon dc MD[18] with pressures of 100 s of Torr and electron density of about 10^{20} m^{-3}. In addition, LTS and diode laser absorption spectroscopy were employed to measure the electron temperature and electron density in an argon dc MD[19] with a driving current of 50 mA and pressure of $300-700$ Torr, in which the electron density was about 10^{19} m^{-3}. However, these optical and laser-aided diagnostics demand complex experimental setups and they also face challenges because of the high collisionality at atmospheric pressure.

Since computer simulations can overcome the experimental challenges, they have become an indispensable alternative for MD diagnostics. Numerical studies of dc MDs can be either based on a fluid model[1,12,20] or on a kinetic model, i.e. the particle-in-cell Monte Carlo col-

lision (PIC- MCC)[21–23] method. Kushner used a two-dimensional (2D) fluid model to study the dynamics of cylindrical, metal-dielectric-metal sandwich argon MDs with sizes of a few hundred μm and pressure of $50-500$ Torr, in which an electron density of about 10^{20} m^{-3} and temperature of several eV were obtained[1]. A one-dimensional (1D) fluid model was also used to study a 250 μm gap dc helium MD at a pressure of 250 Torr[12] as well as a 200 μm gap dc helium MD at atmospheric pressure[20], yielding an electron density of 10^{20} m^{-3} and a temperature of tens of eV at a driving current density of about 10^4 A/m^2. Although fluid models can give important and fruitful information, they assume a Maxwellian velocity distribution, whereas MDs are generally at non-equilibrium and the electron velocity distribution is typically non-Maxwellian. Moreover, for a dc MD it has been reported that fluid simulations could not describe features like kinetic effects, observed in PIC-MCC simulations[22]. Thus, it would be more accurate to use a PIC-MCC model in order to examine the kinetic effects in a dc MD. Choi et al.[21] presented a 1D PIC-MCC simulation of a 200 μm gap dc helium MD at atmospheric pressure, and compared the electron density and temperature between fluid and PIC-MCC models. The breakdown voltage in a dc argon MD with a gap size of $1-100$ μm was also studied very recently, by taking into account field emission by the Fowler-Nordheim equation in a PIC-MCC simulation method[23], and the results of this method will be compared with the breakdown voltage in our simulation by using a secondary electron emission PIC-MCC model. These PIC-MCC simulations[21–23] made use of an explicit PIC model, which is known to be time consuming and to suffer from "self-heating", especially at atmospheric pressure, compared to an implicit PIC method[24–26].

In our previous work, an implicit PIC-MCC method was used to study a rf argon glow MD sustained over a wide range of operating conditions[27]. Three different electron energy distribution functions (EEDFs), i.e., a three temperature hybrid mode, as well as a two temperature mode, were identified at different gaps and voltages. Also the breakdown voltage as a function of gap spacing was examined , which is far away from the Paschen law at atmospheric pressure. However, as the Paschen curve is characteristic for dc discharges, the comparison between the exact values was not meaningful. We might expect important differences between dc and rf MDs at atmospheric pressure. Therefore, in this paper, we use the same PIC-MCC simulation model to compare the rf and dc MDs under the same operating conditions. Subsequently, we study the dc breakdown voltage for a gap spacing of $10-1000$ μm, as well as the plasma kinetic properties such as density, current, EEDF, temperature and electric field, for atmospheric pressure dc argon microplasmas, under various operating conditions of driving voltage ($30-1000$ V) and gap size ($10-1000$ μm), to find out the optimum conditions for potentially industrial applications. The breakdown properties in a very small (0.2 μm gap) dc MD sustained by Fowler-Nordheim field emission, was reported in our recent work[28]. To the best of our knowledge, the atmospheric pressure plasma kinetic properties and the gap size scaling on the breakdown voltage in a dc argon MD sustained by a self-consistent secondary electron emission (SEE) model in a wide range of gap sizes ($10-1000$ μm), has not been studied before with an implicit PIC-MCC model.

II. DESCRIPTION OF THE MODEL

In this paper, we have used a direct implicit PIC-MCC code[24–26]. In this PIC-MCC code scheme, the field equations are obtained from direct summation and extrapolation of the equations of particle motion, a standard MCC procedure is used[29] to account for elastic, excitation and ionization electron-neutral collisions, and for elastic scattering and charge exchange ion-neutral collisions. More specifically, electron impact ionization and excitation from the Ar ground state, and electron-Ar and Ar^+-Ar elastic collisions are accounted for. Since the ionization degree is never larger than 1%, Coulomb collisions are negligible[25]. The cross sections used in this paper are adopted from[30–32]. Our method has been described in detail and tested widely before[25,26]. A dc-voltage source of $10-1000$ V is used to drive the MD. Atmospheric pressure argon gas is used at a temperature of 300 K. The MD is sustained between two parallel plate electrodes separated by a gap of $10-1000$ μm. The PIC-MCC model is self-consistently coupled with the SEE model, assuming a constant ion impact SEE coefficient of 0.1, which is the same as used in a fluid model[1] and PIC-MCC[21] simulations, in order to easily compare our results with the results from literature. As the number of electrons and ions increases rapidly due to the SEE at large driving voltages, a particle merging algorithm is used when the macro particle number exceeds a certain value (typically 400 per cell). The initial electron and ion temperatures are 3 eV and 300 K, respectively.

The SEE process[31] is generally believed to play a key role in sustaining the dc discharge. The SEE coefficients depend on many factors, like the electrode material, the status of the electrode surface (i.e., clean or dirty) and the kind of species and their energy impacting on the electrode[33]. We have studied the effects of different SEE coefficients in both dc and rf microdischarges[32], and we found that if the coefficients are not zero, all results, like the breakdown voltage, the electron and ion densities, the plasma potential, the electron temperature, and the EEDFs, are similar, with only small differences in absolute values. However, if the SEE coefficient is assumed to be zero, no discharge can be sustained. So in all simulations below, we consider only SEE due to ion impact, and we assume the SEE coefficient to be equal to 0.1, which corresponds to a clean stainless steel surface at low ion impacting energy (i.e., up to 100 eV)[32]. Indeed, in that case, the SEE coefficient can be assumed to be constant

for clean cathode surfaces[33].

Although a dc discharge is the simplest case, there are some issues that need special attention[34,35]. The first is the driving method: in simulations of a dc discharge, either a voltage driven[34,36] or a current driven[9] method can be used. In order to make predictions of the breakdown voltage, we need to use the voltage driven method without an external resistance. However, this will lead to an overestimation or underestimation of the current density[35] to some extent. Indeed, the plasma density might gradually increase very slowly even after it reaches (quasi) steady state, due to a positive feedback process in the simulations: a higher plasma density will lead to more secondary electrons due to a higher ion current, and more secondary electrons will lead to a higher density. Hence, it is not straightforward to achieve a satisfying steady state in dc discharge simulations by the PIC-MCC method. Therefore, a common method is to cut off the simulations after some specific time, when the plasma density tends to become stable; this method is also used in many other similar simulations (see e.g.: Refs.[29,34,36–38]). However, we have checked that this method will not affect the properties studied here, by cutting off the simulations after various different times. The second issue is that different superparticle weights might lead to different results, so we have used the particle rezoning method by Lapenta[39] to eliminate this problem.

All simulation results, such as the electron and ion densities and currents, the electron temperature, the plasma potential, the electric field and the EEDFs, will be presented at steady state and averaged by several thousand time steps. Here when the simulations reach steady state, the physical properties, such as the density and the temperature, is nearly constant over time and will only oscillate at small amplitude. Note that because the electron energy distribution function is different from a Maxwellian distribution, the electron temperature means averaged electron energy by convention. The simulation time-step is fixed at 4×10^{-12} s and the gap space is divided into 128 cells. Normally the simulations will run for more than 3×10^5 time-steps.

III. RESULTS AND DISCUSSION

A. Comparison between rf and dc MDs

In order to compare the plasma characteristics between rf and dc MDs, Fig. 1 shows the electron and ion densities in the rf MD at four different times in the rf-cycle (a-d), and in the dc MD (e), as well as the rf time-averaged and dc plasma potential (f), for the same gap spacing of 200 μm and a driving voltage of 100 V (note that this is the amplitude for the rf case with a frequency of 13.56 MHz), at atmospheric pressure. The left side of the figures corresponds to the cathode whereas the right side corresponds to the anode. However, for the rf discharge the cathode and anode are equivalent.

It is easy to see from Fig. 1(a-d) that the rf electron density varies with time, while the rf ion density is nearly constant throughout the whole rf cycle, since the ions cannot follow the rapidly oscillating rf electric field due to their high mass and low mobility. The rf electron density shows asymmetric distributions with a longer sheath on the left side and the right side, respectively, at $\pi/2$ and $\pi 3/2$, whereas, the electron density distribution is symmetric and the same at π and 2π. The dc electron and ion density profiles (Fig. 1(e) are also asymmetric, with their maximum closer to the cathode than to the anode.

The rf peak electron and ion densities (which are the same in the bulk plasma)are 1.1×10^{19} m^{-3} and remains constant as a function of time. Note that the "peak density" means the maximum bulk density for both electrons and ions throughout the paper. The dc peak density is slightly higher, i.e., 1.3×10^{19} m^{-3}. The reason for this is the more efficient electron impact ionization in the dc mode, due to its larger potential drop in the sheath [see Fig. 1(f)], compared to the rf mode, for the same driving voltage and gap spacing. Indeed, the plasma potential drop in the sheaths is 40 V in the rf case, while it is 100 V in the dc case, as shown in Fig. 1(f). Even the accumulated potential drop ($\sim$ 80 V) of the two sheaths in the rf mode is still lower than the dc potential drop ($\sim$ 100 V) in the single sheath. This means that electrons will acquire more energy in the dc sheath than in the rf sheaths in average.

Note that this result is different from the low pressure case ($<$ 300 mTorr), where the rf maximum density is typically larger than in the dc case, if all parameters are the same[40,41]. This is because at atmosphere pressure the Ohmic or collisional heating is the sole heating mechanism. An electron can only gain energy in the sheath with the upper limit of the potential drop in the sheath. On the other hand, at low pressure, collisionless or stochastic heating is dominant[41–43], leading to a much larger density for the rf driven case. In our previous work, the rf MD was studied in detail. In the present paper, a similar detailed study of the dc MD will be presented.

B. Breakdown voltage as a function of gap size

In this section, we will study the breakdown characteristics for dc micro discharges. In our simulations, the breakdown voltage is calculated by the following method: first we fix all the parameters and we vary the voltage over a broad range, in steps of 5 V. Below a specific voltage, the simulations will no longer be sustainable: the plasma density will gradually decrease to zero during the simulations, which means that the plasma cannot be generated or sustained. Above a certain voltage, the plasma density will become stable. The breakdown voltage is given by this specific voltage, which means that the error is at maximum 5 V.

Figure 2(a) presents the calculated breakdown voltage as a function of gap size in the range of $10-1000$ μm. Note that the breakdown voltage is in the order of $\sim 30-75$ V between $10-100$ μm, which is much smaller than the values reported in Ref.[23], i.e., $\sim 550-1000$ V, although the same rising trend with increasing gap size was reported. This is because of different model assumptions. Indeed, in Ref.[23] the MD was assumed to be sustained by field emission, whereas in our simulation the MD is sustained by SEE at all gaps in the range of $10-1000$ μm. Indeed, it has been demonstrated experimentally that the Paschen law is valid for gaps greater than ~ 10 μm, confirming the assumption that field emission has negligible effects on the breakdown voltage considered here[44,45].

The breakdown voltage generally increases with increasing gap size, although it slightly decreases from 75 V at 100 μm to 70 V at 200 μm, This local minimum at 200 μm can be explained by comparing the mean free path for ionization of the SEE electrons with the gap spacing. Indeed, the mean free path of the SEE electrons is around 100 μm in argon at atmospheric pressure. Thus, when the gap spacing is 200 μm, it is larger than the mean free path, and the electron and ion densities show a maximum in the bulk near the sheath in front of the cathode, from which the SEE electrons are generated [see Fig. 4(a) below)], and the latter causes a further increase of this maximum, so the discharge is further enhanced. On the other hand, when the gap spacing is 100 μm, the maximum electron and ion densities appear closer to the anode, where the electrons are completely absorbed, hence a larger breakdown voltage is needed to sustain the plasma in this case, compared to the MD at 200 μm. This minimum breakdown voltage at 200 μm is similar to the normal Paschen law, which has a minimum at about 250 μm for argon[46].

To sustain a stable discharge, the electrons heated in the cathode sheath must produce enough electron-ion pairs by ionization to compensate for the loss of the electrons and ions at the anode. This means that some of the electrons must be heated in the cathode sheath to above the ionization threshold (which is 15.8 eV for argon). When the gap spacing is larger, the electric field is typically lower and the heating process in the cathode sheath can be quite slow, so the electrons must travel a rather long distance to gain energy above the ionization threshold. This means that the electrons on their way can lose a significant amount of energy by excitation, as the mean free path is small compared to the distance travelled by the electrons. However, when the gap spacing becomes comparable or smaller than half of the mean free path of the SEE electrons (hence below 50μm), the electrons will be heated to above the ionization threshold much more quickly, without losing much energy by inelastic collisions, and this significantly increases the efficiency of ionization and thus reduces the breakdown voltage. This explains the local maximum in breakdown voltage for the 100μm gap size. Note that the obtained breakdown voltages in the entire range of discharge gaps ($10-1000$ μm) are quite small (i.e., not larger than 150 V) because the discharge is sustained by SEE. This is beneficial in terms of energy saving considerations.

The peak electron density obtained at the breakdown voltage is plotted as a function of gap size in Fig. 2(b), and the corresponding peak electron current density is presented in Fig. 2(c). The peak electron density decreases very steeply with increasing gap size, i.e., from 1.2×10^{21} m^{-3} at a 10 μm gap to 5.2×10^{19} m^{-3} at a 50 μm gap. Subsequently, it drops more slowly to 4.8×10^{18} m^{-3} at a 500 μm gap due to the lower electric field as well as the lower amount of ionization with increasing gap size, and finally it increases again to 1.3×10^{19} m^{-3} at a 1000 μm gap, because the breakdown voltage now mainly determines the local ionization. The high electron density at the 10 μm gap can again be explained because this gap is much smaller than half of the mean free path of the SEE electrons, so the electrons will be continuously heated in the cathode sheath without losing energy by inelastic collisions, leading to more ionization collisions and this significantly increases the plasma density, compared to the other gaps ($\geq$ 50 m). The peak electron current density has a maximum value of 12651 A/m^2 at the 10 μm gap, and it shows a very similar trend as the electron density, which is logical.

When comparing the breakdown voltage and peak electron density at breakdown voltage with the results obtained in the rf MD[27], it is clear that a similar behavior is observed in both cases. Indeed, in the rf MD a local minimum was observed for the 280 μm gap, and a local maximum at 100 μm. However, the difference between the values of this local minimum and maximum in the rf case was much more pronounced (i.e., 90 vs 50 V, compared to 75 vs 70 V in the dc case; see Fig. 2(a)). This is because in the dc case most electrons and ions are generated and accumulate at a distance smaller than 100 μm from the cathode (see Figs. 4-5), although a small part of the electrons is absorbed by the anode for a discharge gap of 100 μm compared to 200 μm. Thus the breakdown voltage for 100 μm is only a little higher than for 200 μm. In the rf discharge, on the other hand, the electrons which are generated from one electrode can be repeatedly heated by the oscillating rf electric field in the bulk plasma at a gap of 280 μm, because this is larger than twice the SEE electron mean free path, whereas at 100 μm, a much larger number of electrons may be absorbed by the two electrodes, leading to a much higher breakdown voltage for maintaining the discharge at steady state than at 280 μm. In general, however, the values of the breakdown voltage are in the same order in both cases, although in the rf MD the breakdown voltage was never higher than 90 V (which was thus reached at the local maximum of 100 μm). The reason why in the dc MD the breakdown voltage becomes higher than 100 V for gaps larger than 500 μm, can be explained by the rather weak electric field in the longer bulk region compared to the rf case where the electrons are heated by the oscillating rf field. The

behavior and the values of the peak electron density are, very similar in both dc and rf MDs, although the values in the dc case are slightly higher, because of the more efficient electron impact ionization in the dc mode, due to its larger potential drop in the sheath, as shown in Fig. 1(f).

In the next sections, we will illustrate the plasma behavior for three different gap sizes, i.e., 10 μm (corresponding to the conditions of more effective heating of the SEE electrons to above the ionization threshold in the cathode sheath, and hence a very low breakdown voltage), 200 μm (corresponding to the local minimum in breakdown voltage when the gap size is larger than the mean free path for ionization) and 1000 μm (corresponding to the highest value for the breakdown voltage).

C. Effect of driving voltage at a gap of 10 μm

Not only the breakdown voltage but also the plasma kinetic properties are important for practical applications of a MD. In order to illustrate the effect of different voltages (i.e., 50, 100 and 250 V) compared to the breakdown voltage (30 V) on these plasma characteristics, we show in Fig. 3 the electron and ion densities (a), the electric field (b), and the electron temperature (c) as a function of distance from the cathode, as well as the (spatially averaged) EEDF (d), in the 10 μm gap, for these four different voltage cases. The left side of the figures corresponds to the cathode whereas the right side corresponds to the anode. The sheath thickness is evaluated as the region from the cathode to the position at which the electron density is equal to 95% of the ion density.

In Fig. 3(a), the density shows a single ion and electron peak, leading to charge neutrality in the bulk, for the four different driving voltages. In the sheath, the ion density is slightly higher than the electron density, leading to a net positive space charge, as is common in dc glow discharges. The density increases with increasing voltage due to the enhanced ionization, and the peak densities are calculated to be 1.2×10^{21} , 2.1×10^{21} , 1.1×10^{22} and 3×10^{23} m^{-3}, respectively, for 30 V, 50 V, 100 and 250 V. At 30 and 50 V, a relatively large cathode sheath with a width of ~ 6.5 μm, and a much smaller bulk plasma with a width of ~ 3.5 μm are observed, and there is no anode sheath. At 100 V, the cathode sheath is 5.5 μm, the anode sheath is ~ 0.5 μm, and the bulk plasma region is ~ 4 μm, whereas at 250 V, the cathode sheath is 3.9 μm, the plasma bulk region is 5.6 μm and the anode sheath is again ~ 0.5 μm. In other words, the cathode sheath is larger than half of the discharge gap for 30, 50 and 100 V, which is similar to fluid simulations from literature[12] although the electron and ion densities did not give rise to a quasi-neutral plasma in that case. Note that even the high density of $\sim 10^{23}$ m^{-3} in the neutral bulk region is still in the glow discharge limit, as the ionization degree is lower than 1%.

As observed from Fig.3(b), the electric field in the cathode sheath increases rapidly with increasing voltage, and takes a maximum negative value of -7.2×10^6, -1.1×10^7, -3.1×10^7, and -10^8 V/m at the cathode, at 30, 50, 100 and 250 V, respectively. It is interesting to see that the electric field at 250 V has a maximum positive value of 10^7 V/m at the anode, as well as a second maximum of 5×10^5 V/m at the cathode sheath edge.

The electron temperatures exhibit several peaks in the sheath and low values in the bulk plasma, as is clear from Fig. 3(c). This can be understood as follows: the electrons will be continuously accelerated in the dc electric field, so they will accumulate energy, explaining the rise in the temperature profiles, until their energy is above the excitation or ionization threshold, when they can give rise to excitation or ionization collisions, thereby losing their energy, leading to a sharp drop in the temperature profiles. This process can occur several times within the sheath, as long as the dc voltage is high enough, resulting in many peaks of the electron temperature in the sheath. These peaks in the electron temperature are especially obvious at 100 and 250 V, which is logical. At 30 and 50 V, on the other hand, the electron temperature shows an almost linear increase in the cathode sheath with a maximum value at the sheath edge, because earlier in the sheath the electron energy was too low to cause a substantial amount of excitation or ionization, which would lead to sudden drops in the electron temperature. The peak electron temperature values are 0.13, 0.37, 2.41 and 1.81 eV, respectively, for 30, 50, 100 and 250 V. The maximum electron temperature at 250 V is lower than at 100 V, which could be due to the fact that the electrons lose more energy in the sheath, because they give rise to more ionization, as is clear from the much higher electron density (i.e., factor 30 higher at 250 V compared to 100 V; cf. Fig. 3(a)).

In order to examine the electron kinetics in more detail, we plot in Fig. 3(d) the spatially averaged EEDFs, which show a two-energy group distribution for all four voltages, corresponding to a major low-energy (≤ 7 eV) electron group and a minor high energy (> 7 eV) electron group. This is due to the much higher electron density in the bulk region compared to the sheath (see Fig. 3(a)). Furthermore, the Ramsauer-Townsend effect[47] can be clearly seen in the EEDFs, as the electron scattering cross section of argon shows a shallow minimum in the vicinity of 2 eV, so most electrons have an energy around 1.5 eV. In the high energy region (> 7 eV) the electron population almost linearly decreases with increasing energy, because the electrons in the high energy group are continuously heated in the dc electric field in the sheath, but at the same time they will lose energy through excitation or ionization collisions, so the higher energy electron population decreases and only a minority of electrons can accumulate the maximum energy corresponding to the driving voltage (i.e., 30, 50, 100 and 250 eV, respectively) .

To summarize, the calculated maximum electron and ion densities, sheath width, maximum electric field and

maximum electron temperature are presented in Table 1, for 30, 50, 100 and 250 V in the 10 μm gap, as shown.

D. Effect of driving voltage at a gap of 200 μm

To compare the plasma behavior at larger gap spacing, Fig. 4 shows the effect of the driving voltage at a larger discharge gap of 200 μm, on the electron and ion densities (a), electric field (b) and electron temperature (c), as a function of distance from the cathode, as well as on the spatially-averaged EEDFs (d). The lowest voltage of 70 V corresponds to the breakdown voltage.

It is clear from Fig.4(a) that the ion and electron densities are again equal to each other in the bulk, but they now show a peak at the edge between the cathode sheath and the bulk, which is attributed to the important role of ionization by the SEE electrons, which have a mean free path for ionization of about 100 μm (see above). The density increases with increasing voltage due to the enhanced ionization and the peak densities are calculated to be 3.6×10^{18}, 1.3×10^{19} , 1.3×10^{21} and 1.2×10^{22} m^{-3} , respectively, for 70 V, 100 V, 250 and 500V. The cathode sheath width decreases with increasing voltage; it is 75, 58, 41 and 21 μm, respectively, for 70, 100, 250 and 500 V. The anode sheath width is negligible in all cases. In the sheath, there is a significant difference between the electron and ion densities at 70 and 100 V. Indeed, at 70 V, the electron and ion densities are about 10^{15} and 10^{18} m^{-3}, respectively, hence the ion density is three orders of magnitude higher than the electron density. At 100 V, the difference is a bit lower, but still the ion density ($\sim 3\times10^{18}$ m^{-3}) is a factor of 30 higher than the electron density ($\sim 10^{17}$ m^{-3}).

These results agree qualitatively with experimental[17,18] and other simulation[20,21] results. Compared to Ref.[21] for a current driven helium MD (200 μm gap and $\sim$ 250 V), the sheath width in our case is quite similar (i.e., 41 μm compared to $\sim$ 40 μm obtained with the explicit PIC-MCC model and $\sim$ 45 μm obtained with the fluid model in Ref.[21]). However, the density profile is more asymmetric, with a peak near the cathode sheath, and the peak density is almost two orders of magnitude higher. This is because argon can be more easily ionized (lower ionization threshold), leading to a higher plasma density. Moreover, the asymmetric profile is attributed to the lower diffusion in argon than in helium. As we dont know the exact value of the voltage from the current-driven MD in Ref.[21], a direct comparison is impossible. However, our simulations will be useful to compare with future experiments, as the voltage is more easily measured.

As shown in Fig.4 (b), the electric field reaches its maximum negative value again at the cathode. It is -1.7×10^6, -3×10^6 ,-9.8×10^6, and -2.4×10^7 V/m at 70, 100, 250 and 500 V, which is significantly smaller compared to the case of 10 μm, but on the other hand, the region where the field is non-zero is much longer than 10 μm.

As is clear from Fig.4(c), the electron temperatures exhibit again several peaks in the sheath, with a maximum value at the end of the sheath and low values in the bulk plasma, because the electron impact ionization is mainly induced by the SEE electrons from the cathode. The peaks in the sheath are now obvious for all voltages, and they correspond again to energy gain from the electric field, followed by energy loss due to collisions, like in the 10 μm gap (see above). The peak electron temperature values are 4, 4.3, 4.6 and 3.6 eV, respectively, for 70 , 100, 250 and 500 V. Again, the lower value at 500 V may be due to the more abundant ionization collisions, as in the 10 μm gap. In our simulations, the electron temperature is only a few eV, however, an electron temperature of about 20eV is reported in the sheath[21], even above the excitation threshold, which is not likely to occur in atmospheric pressure discharges, because the collisions are so strong that most electrons cannot gain that high energy. We think this phenomenon may be partially attributed to numerical heating in the explicit PIC method, which will numerically heat the electrons and lead to an overestimation of the electron temperature if the space step is not small enough.

In Fig. 4(d), the spatially averaged EEDFs show a three-energy group distribution for all four voltages. We can distinguish a low-energy ($<$ 2 eV), mid-energy (between 2 and 20 eV), and high-energy ($>$ 20 eV) group at 100, 250 and 500 V, while at 70 V, the mid-energy and high-energy groups are between 2 and 12 eV, and $>$ 12 eV, respectively. The majority of electrons is in the low-energy group, due to the much higher electron density in the bulk region (see Fig. 4(a)). The EEDF at 70 V exhibits a Ramsauer-Townsend-like distribution in the low-energy region, with a minimum around 1.2 eV. In the mid-energy region the electron population decreases with higher voltage. Furthermore, at 100, 250 and 500 V, the electron population drops more smoothly with increasing energy in the high-energy region, as the electrons are significantly heated from the cathode to the bulk edge.

Again, the calculated maximum electron and ion densities, sheath width, maximum electric field and maximum electron temperature are summarized in Table 2, for 70, 100, 250 and 500 V in the 200 μm gap.

When we compare the results obtained for the discharge gaps of 10 and 200 μm for the same driving voltage of 100 V, it is clear that the sheath occupies a larger portion in the 10 μm gap, and the electron and ion densities show a relatively broad maximum ($\sim 10^{22}$ m^{-3}) in the bulk, while in the 200 μm gap the sheath is much smaller than the gap size and the electron and ion densities show a peak (which is much lower, i.e., $\sim 10^{19}$ m^{-3}) near the sheath-bulk interface. The reason for the different density profiles (and density values) is that in the small gap of 10 μm the electrons are more efficiently heated, giving rise to more effective ionization in the entire bulk region, explaining the broader density profile and higher density values, whereas in the 200 μm gap, the electrons

are only generated in the bulk near the cathode sheath edge, because the mean free path of the SEE electrons ($\sim$ 100 μm) is smaller than the gap size. In addition, the electron temperature is smaller in the 10m gap than in the 200 μm gap (i.e., $\sim$ 2 eV vs. $\sim$ 4 eV), because the electrons are less effectively accelerated in the significantly smaller sheath ($<$ 6 μm) in the 10 μm gap than in the larger sheath ($\sim$ 60 μm) in the 200 μm gap. This does not contradict the above discussions, as the electron temperature is determined by the average heating for all electrons, which is more effective for larger gap spacing. On the other hand, the minimum breakdown voltage and ionization efficiency are governed by only a small amount of high energy electrons, which is more effective for the smaller gap spacing,

This fact also explains why in the 200 μm gap the EEDF exhibits a three-energy group distribution, whereas a two-energy group distribution is observed in the 10 μm gap. Indeed, this is again due to the small sheath width, i.e., the SEE electrons will be immediately heated to the higher energy electron group before they lose energy by collisions, as the electric field is much larger . It can be clearly seen that there is a significantly larger amount of high energy electrons above the ionization threshold for the smaller gap spacing.

E. Effect of driving voltage at a gap of 1000 μm

Finally, Fig. 5 shows the electron and ion densities (a), electric field (b) and electron temperature (c) as a function of distance from the cathode, as well as the EEDF (d) at four different voltages for the largest gap considered in this work, i.e., 1000 μm. The lowest voltage of 150 V corresponds again to the breakdown voltage.

It is obvious from Fig. 5(a) that the densities now show a narrow peak at the sheath edge with much lower values in the bulk plasma, and the sheaths occupy a very smaller portion of the discharge gap, at rising gap size. Indeed, the absolute sheath width increases from several μm in the 10 μm case (Fig. 3) to tens of μm in the case of the 200 and 1000 μm gaps (Figs. 4 and 5). This is quite logical, because of the high voltages and the large gap spacing, and the small values of the mean free path of the SEE electrons ($\sim$ 100 μm; cf. above). The density increases again with voltage due to the enhanced ionization and the peak densities (again the same for the electrons and ions in the bulk) are calculated to be 1.2×10^{19} , 1.3×10^{21}, 1.3×10^{22} and 2.5×10^{22} m^{-3}, respectively, at 150 V, 250 V, 500 V and 1000 V. In the sheaths, the electron and ion densities are quite different, especially at 150 V, giving rise to a significant positive space charge.

The narrow sheaths ($<$ 45 μm) are also apparent from Fig. 5(b), and the electric field reaches maximum negative values of -5.7×10^6, -2.1×10^7 ,-4.6×10^7, and -6.6×10^7 V/m at 150, 250, 500 and 1000 V. Note that the maximum negative electric field at 250 V is smaller than in the case of 10 μm (cf. Fig. 3(b)), which is logical, as the sheath is thinner in the latter case, so the potential needs to drop over a shorter distance, resulting in a larger electric field. On the other hand, it is larger than the value at 200 μm (cf. Fig. 4(b)), due to the narrower sheath (i.e., 25 μm vs 41 μm in the 200 μm gap; cf above).

We can see from Fig. 5(c) that at 150 V, the electron temperature increases almost linearly in the sheath, and reaches a maximum value of 8.3 eV at the sheath edge, with a low and nearly constant value of $\sim$ 0.7 eV in the bulk plasma. The electron temperature profile at 250 V is similar with that at 150 V, although the electron temperature peak is closer to the cathode and the peak value is 7.7 eV, due do the narrower sheath ($\sim$ 25 μm for 250 V vs $\sim$ 45 μm for 150 V). At 500 and 1000 V, the electron temperature reaches a maximum of 1.5 eV at 14.6 μm in the sheath, and nearly constant values of 1.2 and 0.8 eV in the bulk, respectively. The electron temperatures in the sheath at 500 and 1000 V are lower than at 150 and 250 V. The reason is probably that the electric field in the sheath is much larger for high voltage, so that the electrons can be heated above the ionization threshold within the sheath, leading to significantly electron energy loss by inelastic collisions. This also explains the higher ionization rate and density.

The spatially-averaged EEDFs show again a typical three-energy group distribution, corresponding to low-energy ($<$ 3 eV), mid-energy (between 3 and 10 eV), and high-energy ($>$ 10 eV) electrons at 150 and 250 V, and low-energy ($<$ 4 eV), mid-energy (between 4 and 11 eV), and high-energy ($>$ 11 eV) electrons at 500 V, while a two-energy group distribution, corresponding to low-energy ($<$ 10 eV) and high-energy ($>$ 10 eV) electrons is observed at 1000 V; see Fig. 5(d). It is easy to see that the lower boundary ($\sim$ 10 eV) of the high energy group falls into the energy region between the excitation and ionization thresholds, because the electrons will lose their energy near these energy values. Nevertheless, at all voltages, the majority of the electrons is again in the low-energy region, due to the much higher electron density in the bulk region (see Fig. 5(a)).

When comparing the results between 200 and 1000 μm for the same driving voltage of 250 V, it is clear that the sheath is somewhat smaller at 1000 μm than at 200 μm (i.e., $\sim$ 25 μm vs. $\sim$ 41 μm). Indeed, in the gap of 1000 μm, the electrons and ions are strongly locally distributed and there are almost no species in the bulk region (at a distance from the cathode larger than 150 μm). This local distribution leads to lower losses, and therefore a smaller sheath is sufficient to sustain the discharge. The maximum densities in both gaps are comparable ($\sim 1.6 \times 10^{21}$ m^{-3}). Again, the maximum electron temperature in the sheath is higher in the 1000 μm gap than in the 200m gap (i.e., $\sim$ 8 eV vs. $\sim$ 4.5 eV), due to the stronger electric field in the narrower sheath in the 1000m gap than in the 200 μm gap (see Figs. 4(b) and 5(b)).

When comparing the results among the three different

gaps, i.e., 10, 200 and 1000 μm, for the same driving voltage of 250 V, we can conclude that the peak density is largest for the 10 μm gap, due to the largest electric field (see Fig. 3(b)) yielding more ionization, while the maximum electron temperature increases with rising gap size, because the electrons can be heated over a longer distance in the sheath as the gap size increases, despite the fact that the largest electric field is obtained in the 10 μm gap. Hence, the plasma characteristics for the three gaps studied here are clearly different, and show that an atmospheric pressure argon dc MD exhibits a quite different behavior, depending on the gap size.

IV. CONCLUSION

We have presented a one-dimensional implicit particle-in-cell Monte Carlo collision simulation study of the kinetic plasma properties in an atmospheric pressure d-c argon MD operating in the glow regime in a wide range of driving voltages ($30 - 1000$ V) and gap sizes ($10 - 1000\mu$m). The effect of gap size scaling (in the range of $10 - 1000$ μm) on the breakdown voltage, peak electron density and peak electron current density at the breakdown voltage is examined. The breakdown voltage is found to be lower than 150 V in all gaps considered. This illustrates that dc MDs at atmospheric pressure that are sustained by SEE in the glow regime can be operated in an energy efficient way, which is of crucial importance in terms of energy considerations. The microdischarge is characterized by a neutral bulk plasma region and a cathode sheath region, which fills (more than) half of the discharge gap for a gap size of 10 μm and relatively low discharge voltages, but the ratio of sheath size vs. discharge gap significantly shrinks with increasing gap size and driving voltage, and the sheath becomes even negligible at a gap size of 1000 μm and driving voltages of $500 - 1000$ V.

The calculated bulk electron and ion densities are in the order of $10^{18} - 10^{23}$ m^{-3} at typical conditions, and the electron temperature is typically a few eV in the 10 and 200 μm gap, but it can reach up to 8 eV in the 1000 μm gap at 250 V. Note that even at the high density of $\sim 10^{23}$ m^{-3} the MD is still in the glow discharge limit, as the ionization degree is lower than 1%. The electron energy distribution function (EEDF) shows a two-energy group Ramsauer-Townsend like distribution at a gap of 10 μm, and a three-energy group distribution at the larger gaps of 200 and 1000 μm, emphasizing the importance of the gap spacing effect in dc MDs. From our simulations, it is clear that three different discharge "modes" can be distinguished, depending on the gap spacing, with different characteristics. They might serve as reference values for the basic physics and the experimental design of atmospheric pressure dc MDs.

V. ACKNOWLEDGMENTS

Y. Zhang and W. Jiang gratefully acknowledge the Belgian Federal Science Policy Office and the China Scholarship Council for financial support. The calculations were performed using the Turing HPC infrastructure at the CalcUA core facility of the Universiteit Antwerpen, a division of the Flemish Supercomputer Center VSC, funded by the Hercules Foundation, the Flemish Gov- ernment (department EWI) and the Universiteit Antwerpen.

VI. REFERENCES

* Electronic address: weijiang@hust.edu.cn

[1] Kushner M J 2005 *Journal of Physics D: Applied Physics* **38** 1633 URL http://stacks.iop.org/0022-3727/38/i=11/a=001
[2] Bruggeman P and Brandenburg R 2013 *Journal of Physics D: Applied Physics* **46** 464001
[3] Fridman A, Chirokov A and Gutsol A 2005 *Journal of Physics D: Applied Physics* **38** R1
[4] Schröder D, Burhenn S, Kirchheim D and Schulz-von der Gathen V 2013 *Journal of Physics D: Applied Physics* **46** 464003
[5] Foest R, Schmidt M and Becker K 2006 *International Journal of Mass Spectrometry* **248** 87–102
[6] Park G, Park S, Choi M, Koo I, Byun J, Hong J, Sim J, Collins G and Lee J 2012 *Plasma Sources Science and Technology* **21** 043001
[7] Yokoyama T, Hamada S, Ibuka S, Yasuoka K and Ishii S 2005 *Journal of Physics D: Applied Physics* **38** 1684
[8] Pothiraja R, Ruhrmann C, Engelhardt M, Bibinov N and Awakowicz P 2013 *Journal of Physics D: Applied Physics* **46** 464012
[9] Iza F, Lee J K and Kong M G 2007 *Phys. Rev. Lett.* **99**(7) 075004 URL http://link.aps.org/doi/10.1103/PhysRevLett.99.075004
[10] Marinov I, Guaitella O, Rousseau A and Starikovskaia S 2013 *Journal of Physics D: Applied Physics* **46** 464013
[11] Wang C and Wu W 2013 *Journal of Physics D: Applied Physics* **46** 464008
[12] Kothnur P S, Yuan X and Raja L L 2003 *Applied physics letters* **82** 529–531
[13] Staack D, Farouk B, Gutsol A and Fridman A 2005 *Plasma Sources Science and Technology* **14** 700
[14] Sankaran R M, Holunga D, Flagan R C and Giapis K P 2005 *Nano letters* **5** 537–541
[15] Hensel K, Katsura S and Mizuno A 2005 *IEEE Transactions on Plasma Science* **33** 574–575
[16] Jenkins G and Manz A 2002 *Journal of Micromechanics and Microengineering* **12** N19 URL http://stacks.iop.org/0960-1317/12/i=5/a=401
[17] Wang Q, Koleva I, Donnelly V M and Economou D J 2005 *Journal of Physics D: Applied Physics* **38** 1690
[18] Belostotskiy S G, Ouk T, Donnelly V M, Economou

D J and Sadeghi N 2010 *Journal of applied physics* **107** 053305–053305
[19] Belostotskiy S G, Khandelwal R, Wang Q, Donnelly V M, Economou D J and Sadeghi N 2008 *Applied Physics Letters* **92** 221507–221507
[20] Wang Q, Economou D J and Donnelly V M 2006 *Journal of applied physics* **100** 023301
[21] Choi J, Iza F, Lee J K and Ryu C M 2007 *Plasma Science, IEEE Transactions on* **35** 1274–1278
[22] Hong Y, Yoon M, Iza F, Kim G and Lee J 2008 *Journal of Physics D: Applied Physics* **41** 245208
[23] Radmilovi-Radjenovi M, Matejik, Klas M and Radjenovi B 2013 *Journal of Physics D: Applied Physics* **46** 015302 URL http://stacks.iop.org/0022-3727/46/i=1/a=015302
[24] Lapenta G, Brackbill J U and Ricci P 2006 *Physics of Plasmas* **13** 055904 (pages 9) URL http://link.aip.org/link/?PHP/13/055904/1
[25] Jiang W, Wang H y, Bi Z h and Wang Y n 2011 *Plasma Sources Science and Technology* **20** 035013
[26] Wang H y, Jiang W and Wang Y n 2010 *Plasma Sources Science and Technology* **19** 045023
[27] Zhang Y, Jiang W, Zhang Q and Bogaerts A 2014 *Journal of Applied Physics* **115** 193301
[28] Jiang W, Zhang Y and Bogaerts A 2014 *submitted to Applied Physics Letters*
[29] Nanbu K, Mitsui K and Kondo S 2000 *Journal of Physics D: Applied Physics* **33** 2274 URL http://stacks.iop.org/0022-3727/33/i=18/a=311
[30] Lieberman M A and Lichtenberg A J 2005 *Principles of plasma discharges and materials processing* (John Wiley & Sons)
[31] Furman M and Pivi M 2002 *Physical Review Special Topics-Accelerators and Beams* **5** 124404
[32] Phelps A and Petrovic Z L 1999 *Plasma Sources Science and Technology* **8** R21
[33] Bogaerts A and Gijbels R 2002 *Plasma Sources Science and Technology* **11** 27
[34] Donkó Z, Hartmann P and Kutasi K 2006 *Plasma Sources Science and Technology* **15** 178
[35] Bultinck E, Kolev I, Bogaerts A and Depla D 2008 *Journal of Applied Physics* **103** 013309
[36] Kondo S and Nanbu K 1999 *Journal of Physics D: Applied Physics* **32** 1142 URL http://stacks.iop.org/0022-3727/32/i=10/a=311
[37] Bultinck E and Bogaerts A 2008 *Journal of Physics D: Applied Physics* **41** 202007 URL http://stacks.iop.org/0022-3727/41/i=20/a=202007
[38] Kondo S and Nanbu K 1999 *Plasma Science, IEEE Transactions on* **27** 92 –93 ISSN 0093-3813
[39] Lapenta G 2002 *Journal of computational physics* **181** 317–337
[40] Pan X, Hu B, Ye Y and Kenneth Marcus R 1998 *J. Anal. At. Spectrom.* **13**(10) 1159–1165 URL http://dx.doi.org/10.1039/A805167D
[41] Bogaerts A and Gijbels R 2000 *Spectrochimica Acta Part B: Atomic Spectroscopy* **55** 263–278
[42] Kawamura E, Lieberman M and Lichtenberg A 2006 *Physics of Plasmas (1994-present)* **13** 053506
[43] Sharma S and Turner M M 2013 *Plasma Sources Science and Technology* **22** 035014 URL http://stacks.iop.org/0963-0252/22/i=3/a=035014
[44] Radmilovic-Radjenovic M and Radjenovic B 2007 *Plasma Science, IEEE Transactions on* **35** 1223–1228
[45] Tirumala R and Go D 2010 *Applied Physics Letters* **97** 151502–151502–3 ISSN 0003-6951
[46] Raizer Y P, Kisin V I and Allen J E 1991 *Gas discharge physics* vol 1 (Springer-Verlag Berlin)
[47] Kauppila W, Stein T and Jesion G 1976 *Physical Review Letters* **36** 580

VII. TABLES AND TABLE CAPTIONS

Voltage (V)	Maximum electron and ion density (m^{-3})	Sheath width (μm)	Maximum electric field (V/m)	Maximum electron temperature (eV)
30	1.2×10^{21}	6.3	-7.2×10^{6}	0.13
50	2.1×10^{21}	6.8	-1.1×10^{7}	0.37
100	1.1×10^{22}	5.4	-3.1×10^{7}	2.41
250	3×10^{23}	3.8	-10^{8}	1.81

TABLE I: Calculated maximum electron and ion densities, sheath width, maximum electric field and maximum electron temperature, for a driving voltage of 30, 50, 100 and 250 V and a discharge gap of 10 μm.

Voltage (V)	Maximum electron and ion density (m^{-3})	Sheath width (μm)	Maximum electric field (V/m)	Maximum electron temperature (eV)
70	3.6×10^{18}	75	-1.7×10^{6}	4
100	1.3×10^{19}	58	-3×10^{6}	4.3
250	1.3×10^{21}	41	-9.8×10^{6}	4.6
500	1.2×10^{22}	21	-2.4×10^{7}	3.6

TABLE II: Calculated maximum electron and ion densities, sheath width, maximum electric field and maximum electron temperature, for a driving voltage of 70, 100, 250 and 500 V and a discharge gap of 200 μm.

VIII. FIGURES AND FIGURE CAPTIONS

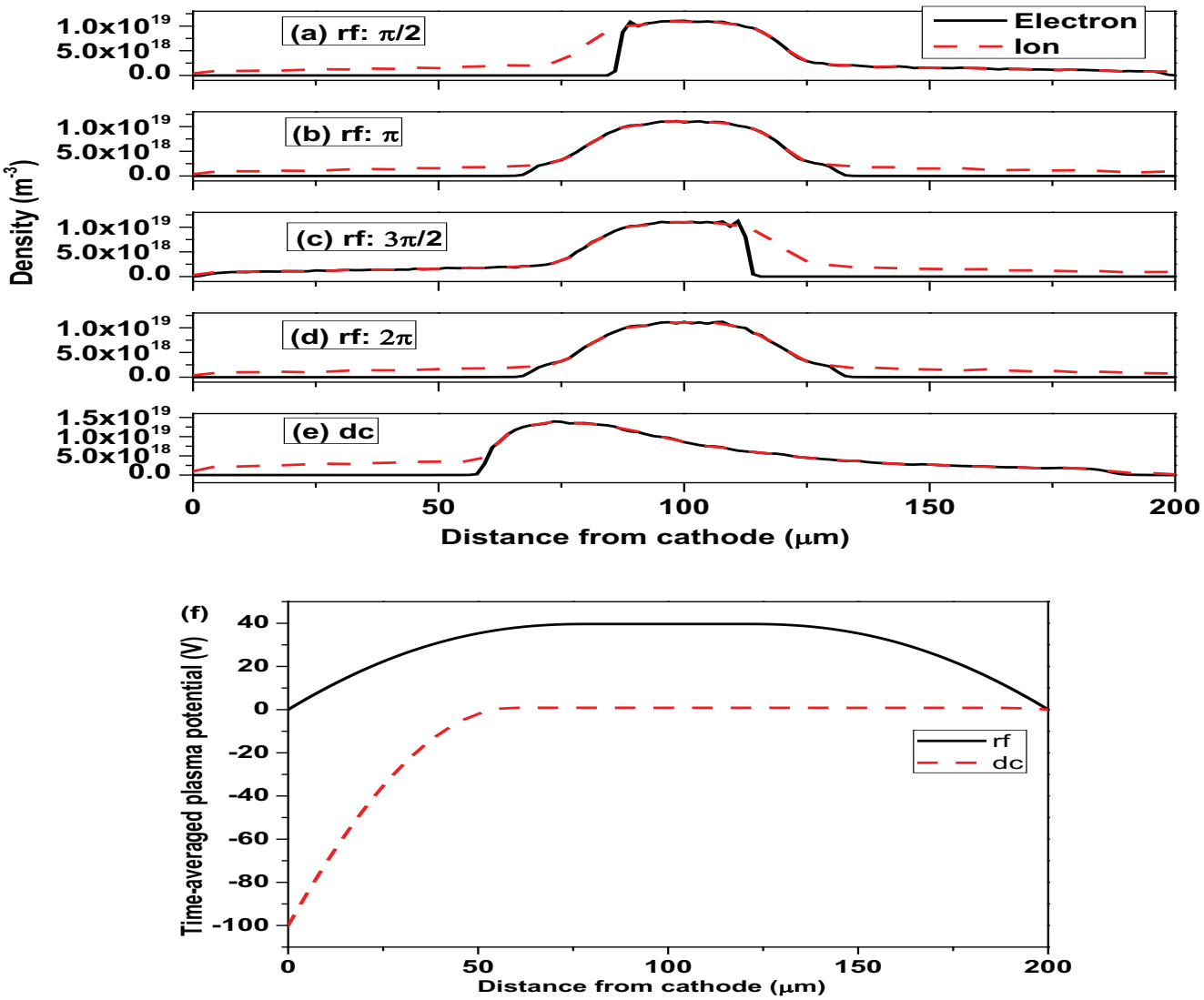

FIG. 1: (Color online) Electron and ion densities in the rf case, at four different times in the rf cycle (a-d) and in the dc case (e), and the time-averaged plasma potential (f) in the rf (solid line) and dc (dashed line) discharges, as a function of distance from the cathode, in a discharge gap of 200 μm for a driving voltage of 100 V.

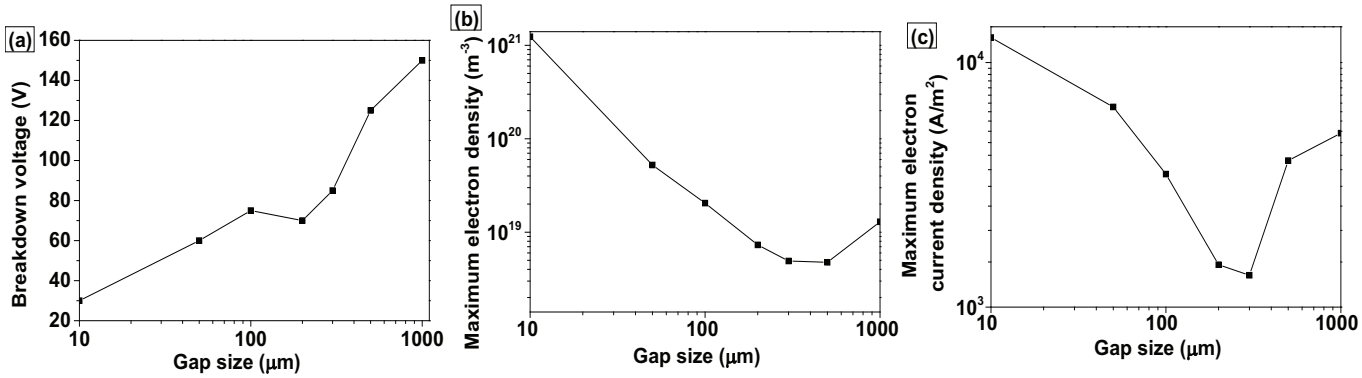

FIG. 2: (Color online) Breakdown voltage (a), peak electron density (b) and peak electron current density (c) at this breakdown voltage, as a function of gap size.

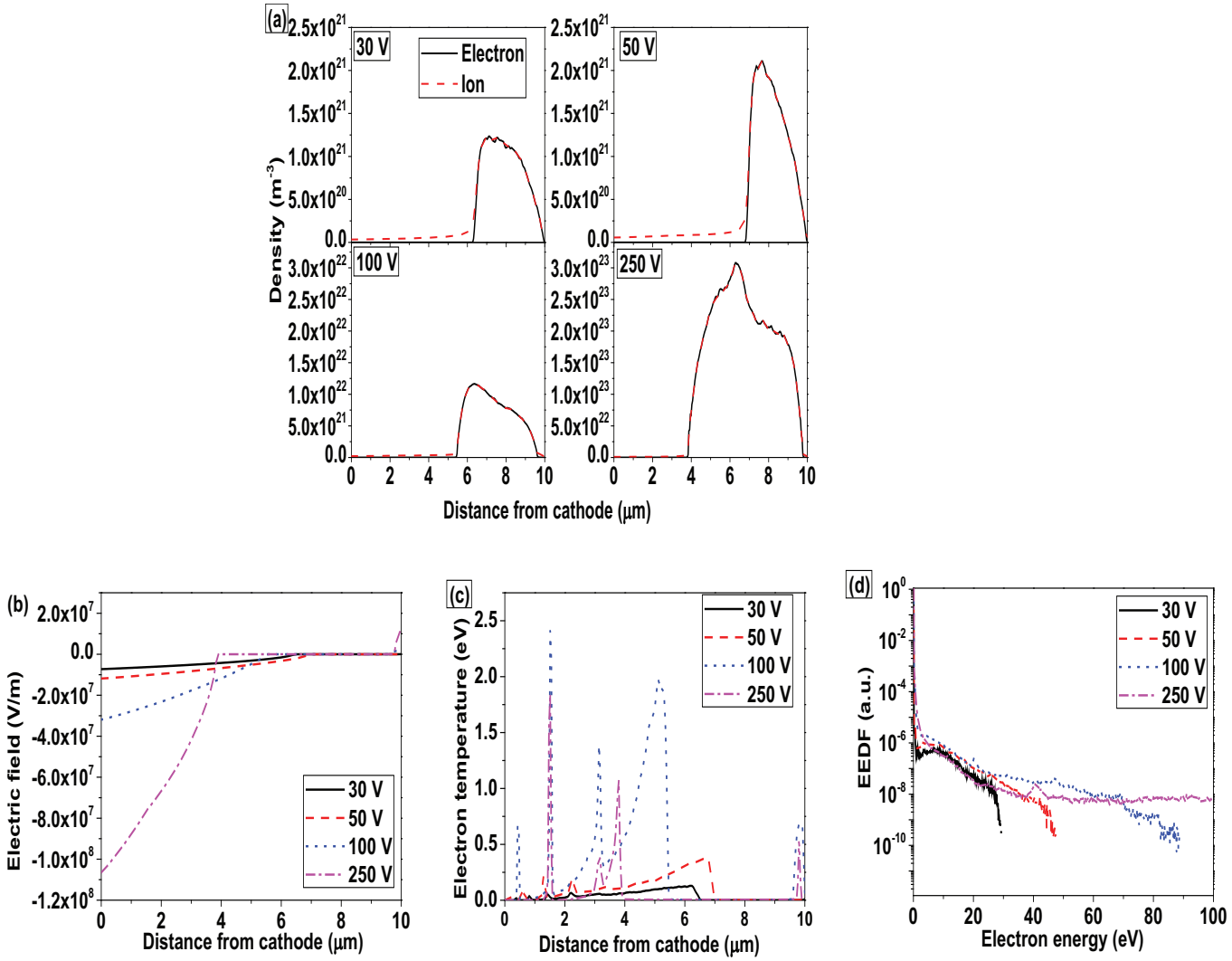

FIG. 3: (Color online) Electron and ion densities (a), electric field (b), and electron temperature (c), as a function of distance from the cathode , and spatially-averaged electron energy distribution functions (EEDFs) (d) , for different applied voltages, in a discharge gap of 10 μm.

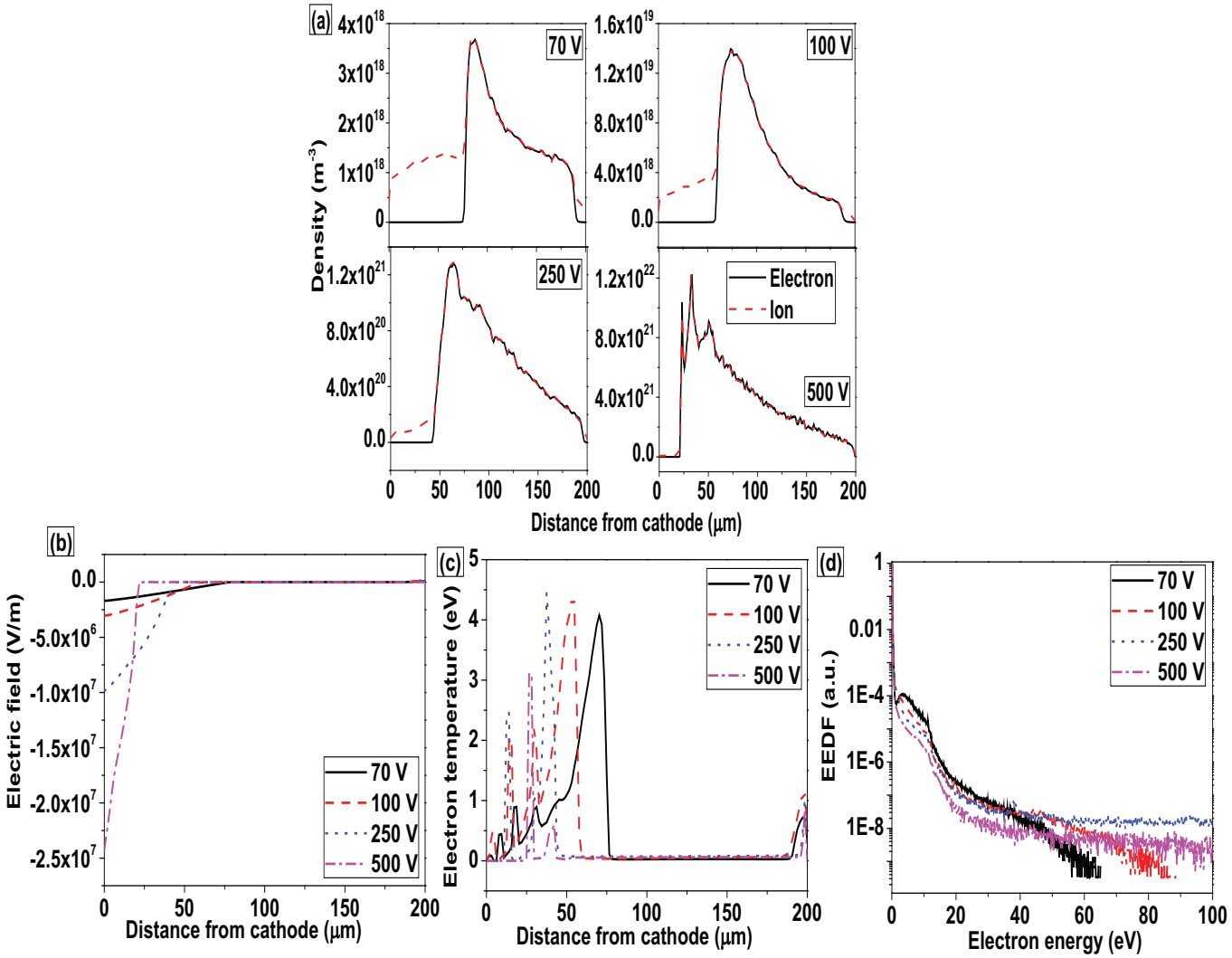

FIG. 4: (Color online) Electron and ion densities (a), electric field (b) and electron temperature (c), as a function of distance from the cathode, and spatially-averaged EEDFs (d), for different applied voltages, in a discharge gap of 200 μm.

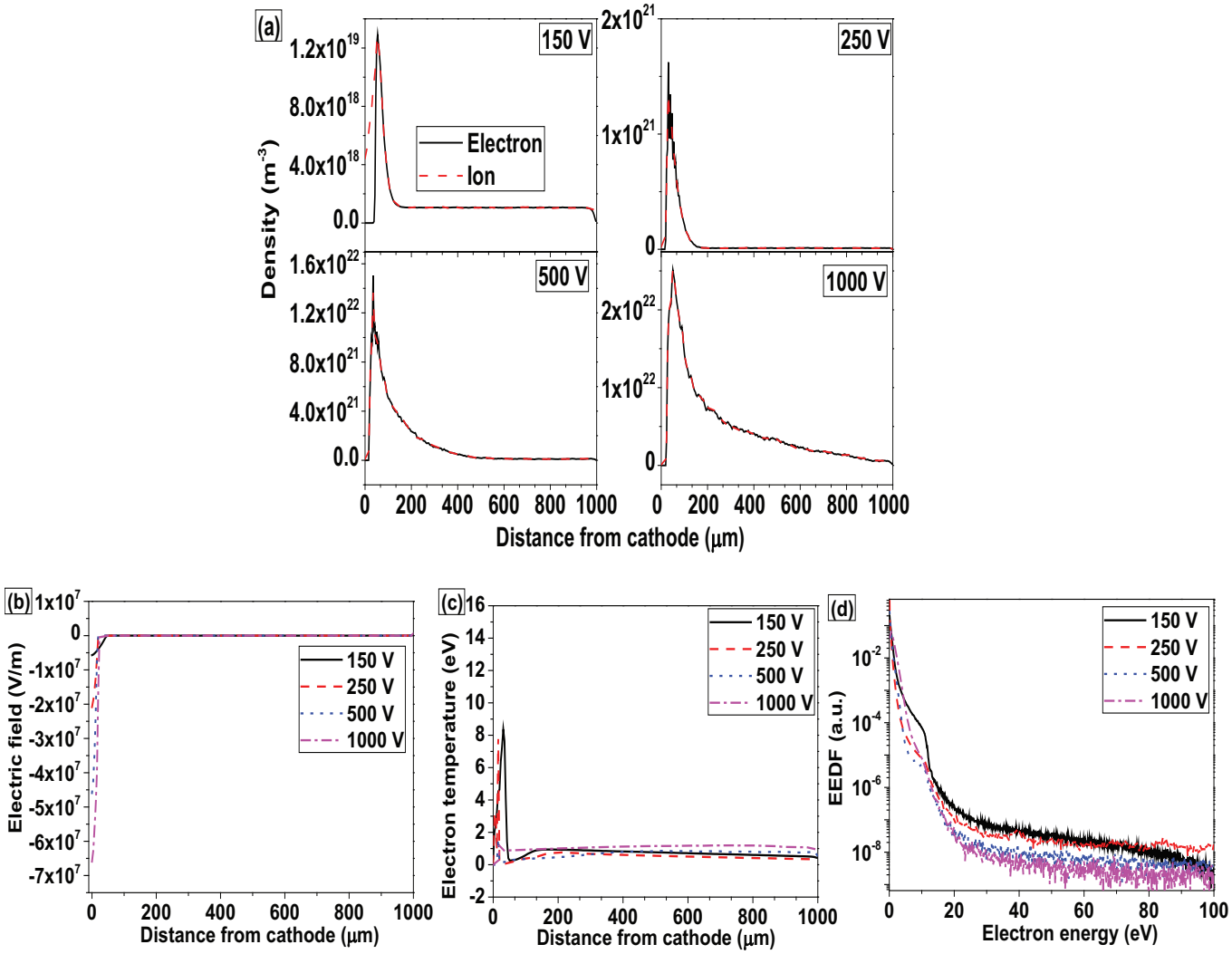

FIG. 5: (Color online) Electron and ion densities (a), electric field (b) and electron temperature (c), as a function of distance from the cathode, and spatially-averaged EEDFs (d), for different applied voltages, in a discharge gap of 1000 μm.